A stable hepatitis D virus-producing cell line for host target and drug discovery

Charlotte Bach, Julie Lucifora, Marion Delphin, Laura Heydmann, Margaux Heuschkel, Caroline Pons, Kaku Goto, Els Scheers, Catherine Schuster, David Durantel, et al.

A stable hepatitis D virus-producing cell line for host target and drug discovery

Charlotte Bach [1,†], Julie Lucifora [2,†], Marion Delphin [2], Laura Heydmann [1], Margaux Heuschkel [1], Caroline Pons [2], Kaku Goto [1], Els Scheers [3], Catherine Schuster [1], David Durantel [2], Frederik Pauwels [3], Thomas F. Baumert [1,4], Eloi R.Verrier [1,*]

[1] Université de Strasbourg, Inserm, Institut de Recherche sur les Maladies Virales et Hépatiques UMR_S1110, Strasbourg, France.
[2] CIRI - Centre International de Recherche en Infectiologie, Univ Lyon, Université Claude Bernard Lyon 1, Inserm, U1111, CNRS, UMR5308, ENS Lyon, F-69007 Lyon, France.
[3] Janssen Research & Development, Janssen Pharmaceutical Companies, Beerse, Belgium.
[4] Institut Hospitalo-Universitaire, Pôle Hépato-digestif, Nouvel Hôpital Civil, Strasbourg, France.
* Correspondence: e.verrier@unistra.fr
† These authors equally contributed to this work.

Abstract: Chronic hepatitis D is the most aggressive form of chronic viral hepatitis. It is caused by super-infection of hepatitis B virus (HBV)-infected hepatocytes with hepatitis D virus (HDV). While the recent conditional approval of bulevirtide for HDV treatment offers a new therapeutic modality in Europe, there is an unmet medical need to further improve therapy. A more detailed characterization of virus-host interactions is needed for the identification of novel therapeutic targets. Addressing this need, we engineered a new stably-transformed cell line, named HuH7-2C8D, producing high titer recombinant HDV and allowing the study of viral particles morphogenesis and infectivity. Using this culture system, where viral propagation by re-infection is limited, we observed an increased accumulation of edited version of the viral genomes within secreted HDV viral particles over time that is accompanied with a decrease of viral particles infectivity. We confirmed interaction of HDV proteins with a previously described host factor in HuH7-2C8D cells and additionally showed that these cells are suitable for co-culture assays with other cell types such as macrophages. Finally, the use of HuH7-2C8D cells allowed to confirm the dual antiviral activity of farnesyl transferase inhibitors, including the clinical candidate lonafarnib, against HDV. In conclusion, we have established an easy-to-handle cell culture model to investigate HDV replication, morphogenesis, host interactions. HuH7-2C8D cells are also suitable for high-throughput antivirals screening assays for the development of new therapeutic strategies.

Keywords: Hepatitis D virus; virus-host interactions; cell culture model; lonafarnib

INTRODUCTION

Hepatitis D virus (HDV) is a small defective virus capable of infecting human hepatocytes and responsible for the more severe form of chronic viral hepatitis (Lucifora and Delphin, 2020). HDV is a satellite virus of hepatitis B virus (HBV), the leading cause of hepatocellular carcinoma (HCC) worldwide, and needs the presence of HBV envelope proteins (HBsAg) for the assembly of new viral particles (Lucifora and Delphin, 2020; Sureau and Negro, 2016). Detected in about 10% of the 296 million patients chronically infected by HBV, HDV infection leads to an accelerated development of liver damage and an increased risk of developing advanced liver disease and HCC compared to HBV mono-infected patients (Sureau and Negro, 2016). Despite the recent development of innovative antiviral therapies based on the administration of the entry inhibitor bulevirtide (Urban et al., 2021), the current long-term treatments involving pegylated interferon alpha (PEG-IFNα) lead to a limited rate of viral clearance (Turon-Lagot et al., 2020). Thus, new therapeutic strategies are needed to further defeat this global health threat. HDV does not encode viral enzymes and thereby relies on host ones. The sole enzymatic activity of HDV is a difficult-to-target ribozyme activity. Targeting host activities compulsory for viral replication is therefore an area that may offer new opportunities. This is demonstrated by the development of lonafarnib, a farnesyl transferase inhibitor (FTI) impairing virion assembly, currently evaluated in phase III clinical trial, and bulevirtide, which targets the virus receptor at the hepatocyte cell surface and received a conditional approval in the European Union (Turon-Lagot *et al.*, 2020; Urban *et al.*, 2021). Targeting host-dependency factors requires extensive knowledge on virus-host interactions and a comprehensive characterization of host factors involved in the viral life cycle. Although the main steps of the HDV life cycle have been characterized, the underlying molecular mechanisms of hepatocyte-HDV interactions still need to be more deeply investigated. HDV is characterized by a small circular RNA genome associated to the two forms of the HDV antigen (HDAg) within the viral ribonucleoprotein (RNP) (Sureau and Negro, 2016). The viral envelope is composed of the three forms of HBV surface antigen (HBsAg) (Sureau and Negro, 2016). Sharing the same envelope proteins, HDV and HBV are likely to enter the cells through a similar mechanism (reviewed in (Herrscher et al., 2020b)), involving the initial attachment to heparan sulfate proteoglycan (HSPG) and a specific binding to the viral receptor NTCP at the hepatocyte basolateral membrane (Ni et al., 2014; Schulze et al., 2007; Verrier et al., 2016a; Yan et al., 2012). NTCP directly interacts with the preS1 region of large HBsAg (L-HBsAg) and this interaction is inhibited by synthetic preS1 peptides such as bulevirtide (Urban *et al.*,

2021). Upon internalization, probably through clathrin-mediated endocytosis (Herrscher et al., 2020a), HDV RNP is released in the cytoplasm and addressed to the nucleus. HDV replication takes place in the nucleus and fully relies on host polymerases, mainly RNA polymerase II (Lucifora and Delphin, 2020). HDV genome serves as a template for the transcription of HDAg mRNA, leading to the production of small HDAg (S-HDAg) that induces viral replication. In parallel, the antigenome is synthetized from HDV genome via a rolling-circle mechanism (Lucifora and Delphin, 2020; Sureau and Negro, 2016). The antigenome in turn serves as a matrix for the production of new versions of the HDV genome through the same mechanism. During viral replication, the adenosine deaminase ADAR edits the antigenome at the mRNA AMBER stop codon site, leading to the transcription of a longer mRNA and the synthesis of the large HDAg (L-HDAg). L-HDAg prenylation, inhibited by FTIs including lonafarnib, triggers both the inhibition of viral replication and virion assembly through the interaction with the small HBV envelop protein S-HBsAg (Lucifora and Delphin, 2020; Sato et al., 2004; Sureau and Negro, 2016; Turon-Lagot *et al.*, 2020). Importantly, viral assembly and release are still poorly characterized.

The understanding of molecular interactions between HDV and hepatocyte host factors has been limited for a long time by the absence of easy-to-use cell culture models (Heuschkel et al., 2021). Although recent advances based on NTCP-expressing cells have allowed significant progress in the past ten years (Heuschkel *et al.*, 2021), key aspects of the viral life cycle, notably assembly and release, remain unclear. Here, we report the establishment of a new HDV-producing cell line, termed HuH7-2C8D, allowing both the production of large stock of recombinant virus and the study of viral replication, assembly and release. We also suggest its use for the screening of host factors and antiviral molecules.

MATERIAL AND METHODS

plasmids and reagents

The lentiviral vector pLX304-HB2.7 expresses HBsAg (Genotype D, serotype ayw, GenBank: V01460.1) and was kindly provided by Professor Stephan Urban (University Hospital Heidelberg, Heidelberg, Germany) (Lempp et al., 2019). The lentiviral vector pLV[shRNA]-Puro-U6>(shHBsAg-1) expresses a shRNA specifically targeting HBsAg (referenced as shHBs in the study) as well as the puromycin resistance gene and was obtained from VectrorBuilder (vector ID: VB220325-1130fza). Target sequence: TTCCAGGATCCTCAACAAC. The lentiviral vector pLV[shRNA]-Puro-U6>Scramble_shRNA#1 expresses a shRNA (shCtrl in the study) with no target sequence in the human

transcriptome and was obtained from VectorBuilder (vector ID: VB010000-0005mme). Target sequence: CCTAAGGTTAAGTCGCCCTCG. The HDV-encoding plasmid pSVLD3 (genotype 1, GenBank: M21012.1) was kindly provided by Doctor John Taylor (Fox Chase Cancer Center, Philadelphia, PA, USA). The production of pSLVD3-neo was adapted from (Chen et al., 1990). A neomycin resistance cassette was inserted into the pSVLD3 plasmid. The sequences of the neomycin resistance gene and its promoter were amplified from EX-C0391-Lv151 (GeneCopoeia) using the following primers: SacI-hPGK_Prom-F: 5′-AAAGAGCTCGGGGTTGGGGTTGCGCCTTTTCCAAG-GCAG-3′ and BamHI-NeoR-R: 5′-AAAGGATCCTCAGAAGAACTCGTCAAGAAGGCGATAG-3′, and subcloned into pSVLD3 upon digestion by SacI and BamHI, producing pSVLD3-neo. Neomycin resistance gene expression is under the control of hPGK promoter (see Figure S1). Lipopolysaccharide (LPS) was obtained from Invivogen (San Diego, CA, USA) and GM-CSF from R&D System. FTI-277 trifluoroacetate salt (F9803), lonafarnib (SML1457), Dimthyl sulfoxide (DMSO), and PEG 8000 (polyethylene glycol) were obtained from Merck. PreS1 peptide is derived from the preS1 region of HBV envelope protein and was synthetized by Bachem (Bubendorf, CH). DNA transfection at the indicated concentrations was performed using the CalPhos Mammalian Transfection Kit (Clonetech) and FuGENE® HD Transfection Reagent (Promega) according to the manufacturers' instructions.

Cell lines

Human embryonic kidney 293T- (HEK 293T) (Lupberger et al., 2011), HepaRG- (Alfaiate et al., 2016; Gripon et al., 2002), and HuH7.5-NTCP cells (Verrier et al., 2022) were cultured and differentiated as previously described. Monocytes purified from blood bags of healthy donors (Etablissement Français du Sang, EFS; code 895/1052) were isolated and cultivated as described (Delphin et al., 2021). For the production of NTCP-overexpressing HuH7, cells were seeded in six-well plates at 50% confluence 1 day prior to transduction with *SLC10A1*-expressing vesicular stomatitis virus pseudoparticles (VSVpp) (GeneCopoeia, 217EX-C0391-Lv151) produced in HEK 293T by transfection as described (Lupberger *et al.*, 2011; Verrier *et al.*, 2016a). After 3 days, cells were expanded and selected for NTCP expression with 500 µg/mL of neomycin (G418). HuH7-NTCP cells were maintained at a concentration of 250 µg/mL G418. For the production of a stable cell line producing HDV infectious particles, HuH7 cells were transduced with VSVpp containing pLX304-HB2.7 and selected with blasticidin at 8 µg/mL, producing the stable cell pool HuH7-HB2.7. Single cell sorting using a cell sorter SH800 (Sony) isolated cell clone

HuH7-2C8 according to intracellular and extracellular HBsAg expression, as quantified by flow cytometry and chemiluminescence immunoassay (CLIA), respectively (see below). Subsequently, HuH7-2C8 cells were transfected with pSVLD3-neo and selected with G418 at 750 µg/mL in presence of blasticidin at 8 µg/mL, producing the HuH7-2C8D cell line. HuH7-2C8D cells were maintained at a concentration of 250 µg/mL G418 and 7 µg/mL blasticidin. The cell line was amplified and stored five passages after transfection with pSVLD3-neo plasmid.

Characterization of HuH7-2C8 and HuH7-2C8D cell lines.

Extracellular HBsAg expression was quantified by chemiluminescence immunoassay (CLIA, Autobio, CL0310-2) according to the manufacturer's instructions. Intracellular expression of HBsAg in the different cell lines was assessed by flow cytometry as described (Eller et al., 2020) using a specific mouse monoclonal anti-HBsAg antibody (clone 1044/329, Novus) and a secondary AF647-labeled goat antibody targeting mouse IgGs (Jackson ImmunoResearch, 115-605-003). A CytoFLEX cytometer (Beckman Coulters) was used. Intracellular HBsAg and HDAg levels were also assessed by Western blot as described (Eller *et al.*, 2020; Verrier *et al.*, 2016a). Briefly, proteins were separated and blotted by electrophoresis and transfer system (BioRad). HBsAg and HDAg expressions were assessed using a monoclonal antibody targeting HBsAg - and a rabbit polyclonal anti-HDAg antibody, respectively. Both antibodies were provided by Janssen Pharmaceutica (Beerse, Antwerp, Belgium). Peroxidase-conjugated goat secondary antibodies targeting human IgGs (109-035-003) and rabbit IgGs (101-035-144) were obtained from Jackson ImmunoResearch. β-actin- or β-tubulin expression was assessed in parallel using a mouse monoclonal antibody (Sigma, A5441) or a rabbit polyclonal antibody (GenTex, GTX101279), respectively. For β-actin detection, a secondary peroxidase-conjugated sheep antibody targeting mouse IgGs (GE Healthcare, NA931) was used. Protein expression was assessed using the ChemiDoc™ Imaging System (BioRad). The interaction between HDAg and MOV10 was assessed by co-immunoprecipitation as previously described (Verrier et al., 2020). HDAg immunoprecipitation was performed using Pierce™ Crosslink Magnetic IP/Co-IP Kit as described (Verrier *et al.*, 2020). Briefly, confluent cells were washed with cold PBS and lysed in ice-cold IP Lysis/Wash Buffer on ice. Lysate was cleared by centrifugation at 13,000 x g for 10 minutes. Cleared cell lysate was incubated with 5 µg of patient-derived anti-HDAg antibody (Verrier *et al.*, 2020) covalently bound to Pierce Protein A/G Magnetic Beads, or 5 µg of human control IgG used as negative control. The beads were washed

extensively to remove non-bound material and bound proteins were eluted in a low-pH elution buffer according to manufacturer's instructions. Eluted samples were separated by sodium dodecyl sulfate–polyacrylamide gel electrophoresis and analyzed by immunoblot using a mouse monoclonal anti-MOV10 (Abcam, ab176687) antibody or the patient-derived anti-HDAg antibody (Verrier *et al.*, 2020).

Production of recombinant HDV infectious particles

For the production of recombinant HDV infectious particles, HuH7-2C8D cells were plated in proliferation medium for three days consisting in HuH7 cell culture medium as described (Eller *et al.*, 2020; Verrier *et al.*, 2016a; Verrier *et al.*, 2020) complemented with 7 µg/mL blasticidin and 250 µg/mL G418. After three days, medium was replaced by production medium. Two types of production medium were used, showing a similar productivity: 1) William's E medium complemented with 10% fetal bovine serum (FBS), penicillin (100 units/mL), and streptomycin (100 µg/mL) or 2) primary hepatocyte maintenance medium (PMM, based on William's E medium (Eller *et al.*, 2020; Verrier *et al.*, 2020)) complemented with 10% FBS. Both media were complemented with 2% DMSO. Cell supernatants were harvested at different time points post medium change for the characterization of HDV infectious particles. Extracellular HBsAg expression was quantified by CLIA. For detection of extracellular HBsAg and HDAg expression by Western blot, supernatant from HuH7-2C8D cells was concentrated 7X with a 30% sucrose cushion after ultracentrifugation at 40,000 rpm for 4 hours at 4°C. Protein expression was assessed as described above. For the quantification of HDV RNA in cell supernatant, total RNA was extracted using ReliaPrep™ RNA Miniprep System (Promega) or NucleoSpin 96 RNA (Macherey Nagel). Reverse transcription was performed using Maxima™ H Minus cDNA Synthesis Master Mix (ThermoFisher Scientific, M1682). qPCR was performed using iTaq Universal SYBR Green Supermix (Bio-Rad) and the following primers: HDV-Fw: 5'-CGGGCCGGCTACTCTTCT-3'; HDV-Re: 5'-AAGGAAGGCCCTCGAGAAC-3'. Absolute HDV cDNA copies were assessed through a quantification standard based on synthetic HDV RNA obtained as described (Alfaiate *et al.*, 2016) or from a quantified specific PCR product obtained from the pSVLD3 plasmid. The quantity of viral particles was estimated based on the quantification of extracellular HDV RNA copies, and was expressed as viral genome equivalents (Vge). For the characterization of viral particles, supernatant from HuH7-2C8 and HuH7-2C8D cells were concentrated with a 30% sucrose cushion and purified through a 10-45% iodixanol density gradient using Optiprep Density Gradient Medium (Merck, D1556) according to manufacturer's

instructions after ultracentrifugation at 40,000 rpm for 16 hours at 4°C. Ten fractions were collected. 200 µL of each fraction were weighted to assess the density. HBsAg levels in each fraction were assessed by CLIA. HDV RNA levels in each fraction were quantified by RT-qPCR as described above. For the silencing of HBsAg expression, HuH7-2C8D cells were seeded one day prior to transduction with a lentiviral vector expressing shHBs or shCtrl. 3 days after transduction, cells were selected in production medium supplemented with puromycin at 1.8µg/mL for 3 days. Puromycin was then removed, and cells were cultured in production medium for 4 days. Supernatants were then harvested and silencing efficacy was assessed by CLIA quantification of extracellular HBsAg. For the inhibition of HDV assembly, HuH7-2C8D cells were seeded in amplification medium. After 3 days, medium was replaced by production medium complemented with FTI-277 at 10µM. Medium was replaced with fresh compound every 2/3 days. Viral parameters were assessed at different time points post treatment as described above.

HDV infection and coinfection.

Infectious virus particles were harvested from the supernatant of HuH7-2C8D cells or produced as described (Alfaiate *et al.*, 2016). If necessary, supernatants were subjected to overnight precipitation with 8% PEG 8000 as described (Alfaiate *et al.*, 2016). HuH7-NTCP cells were infected with recombinant HDV particles as previously described (Verrier *et al.*, 2016a; Verrier et al., 2016b; Verrier *et al.*, 2020). Briefly, HuH7-NTCP cells were seeded one day prior to pretreatment or not with preS1 peptide at 200nM for one hour at 37°C. Cells were then infected by HDV at 100 Vge/cell except otherwise stated in presence of 4% PEG. 16 hours after inoculation, virus was removed, cells were washed and cultured in PMM with 2% DMSO. HDV infection was assessed at 6 days post infection (dpi) by immunofluorescence (IF) using the previously described anti-HDAg rabbit antibody and Alexa Fluor 647-labelled secondary antibody targeting rabbit IgGs (Jackson ImmunoResearch, 111-605-144). Cell nuclei were stained with DAPI. Fluorescent imaging was performed using an Axio Vert.A1 microscope (Carl Zeiss), and the number of HDAg-positive cells was quantified using a Celigo plate cytometer (Nexcellom). Alternatively, Cells were lysed at 6dpi and total RNA was purified as described above. HDV infection levels was assessed by RT-qPCR quantification of HDV RNA primers and TaqMan® probe: HDV-835-851: 5'-TGGACGTGCGTCCTCCT-3'; HDV-905-889: 5'-TCTTCGGGTCGGCATGG-3'. HDV-Pr-856-870: 5'-[FAM]-ATGCCCAGGTCGGAC-[BHQ1]-3'. All values were normalized to *GAPDH* expression quantified using Human GAPD (GAPDH) Endogenous Control (VIC™/MGB probe, primer limited, Applied

Biosystems™, 4326317E). HuH7.5-NTCP and HepaRG cells were infected as previously described (Alfaiate *et al.*, 2016; Verrier *et al.*, 2022), and HDV infection was assessed after 6 days by RT-qPCR quantification of HDV RNA as described (Alfaiate *et al.*, 2016; Verrier *et al.*, 2022). HuH7.5-NTCP cells were coinfected with HBV and HDV as previously described (Verrier *et al.*, 2022).

RT-digital droplet PCR (RT-ddPCR) assay for the quantification of HDV RNA

The RT-ddPCR assay has been extensively described (Verrier *et al.*, 2022). Briefly, total RNAs were purified and reverse transcribed from HuH7-2C8D cell supernatant at different time points post medium change as described above. Edited and non-edited versions of HDV RNA were quantified in a duplex assay through QX200 AutoDG Droplet Digital PCR System (Bio-Rad) according to the manufacturer's instructions as described (Lebosse et al., 2020; Verrier *et al.*, 2022). The following primers amplifying the editable region of the HDV genome were used: HDV_951-970_Fw: 5'-TATTCACTGGGGTCGACAAC-3' ; HDV_1101-1082_Re: 5'-CTTCGTCCCCAATCTGCAG-3'. The dual-labelled probes specific for non-edited and edited HDV sequences were respectively:

HDV_Probe-S : 5'-[6FAM]-CCTATGGAAATCCCTGGTTTCCCCTGATG-[BHQ1]-3'

HDV_Probe-L : 5'-[HEX]-CCCATGGAAATCCCTGGTTTCCCCTGATG-[BHQ1]-3'

Fluorescent data were analyzed using the QuantaSoft analysis software (Bio-Rad). The quantification of absolute sample concentration was obtained by applying Poisson's distribution.

Monocyte co-culture with HuH7-derived cells

Co-culture with HuH7-derived cells was performed as previously described: (Delphin *et al.*, 2021). Briefly, HuH7, HuH7-2C8, or HuH7-2C8D cells were seeded in 24-well plates. Monocytes were seeded into 6.3 mm diameters PET inserts for 24-well plates, with pores of 0.45 uM diameter (Dutscher, 2515127) displayed above HuH7-derived cells (transwell system). Using GM-CSF (50ng/mL), monocytes were differentiated into M1-monocyte-derived macrophages (MDM) through a six-day process, as described (Delphin *et al.*, 2021). M1-MDM were then stimulated with 10 ng/mL of LPS for 3 hours. IL-6 and IL-1β secretions within the M1-MDMs supernatant at day 7 were assessed using DuoSet ELISA from R&D Systems following the manufacturer's instructions.

Statistical analyses.

Results are expressed as means ± standard deviations (SD) as stated in the Figure Legends. Statistical analyses were performed using a two-tailed Mann-Whitney U test; $p < 0.05$ (*), $p < 0.01$ (**), and $p < 0.001$ (***) were considered statistically significant. Significant *p*-values are indicated by asterisks in the individual figures and figure legends. The number of tested biological replicates (n) is indicated in the figure legends.

RESULTS

Production of a stable cell line expressing both HBsAg and the HDV genome

We produced an HuH7-derived cell line stably secreting HDV infectious particles using the strategy depicted in Figure 1A. First, HuH7 cells were transduced with a lentiviral vector expressing a 2.7kb subgenomic fragment of the HBV ayw genome, allowing the expression of S-, M- and L-HBsAg under the control of their native promoters and enhancers (Lempp *et al.*, 2019; Sureau et al., 1994). Transduction efficacy in the HuH7-HB2.7 cell pool was assessed by quantification of HBsAg intracellular expression by flow cytometry. As shown in Figure 1B, only a fraction of the cells expressed HBsAg in the cell pool. In order to select an HBsAg-expressing clone, HuH7-HB2.7 single cells were dispensed in 96-well plates using a cell sorter and single clones were expanded. Among them, the HuH7-2C8 clone was selected according to its robust intracellular HBsAg expression level as determined by flow cytometry (Figure 1B) and HBsAg secretion level as determined by CLIA (Figure 1C, S2). HuH7-2C8 cells were then transfected with pSVLD3-neo plasmid (Figure 1A) that is derived from the HDV genotype 1-expressing plasmid pSVLD3, in which a neomycin resistance cassette was inserted (Figure S1). The resulting cell line, named HuH7-2C8D, was therefore selected for neomycin resistance. As shown in Figure 1B-C, intracellular and secreted HBsAg levels are similar in HuH7-2C8D cells and their parental clone. To characterize the production of HDV particles, HuH7-2C8D cells were seeded and the dynamic of viral protein production was assessed by Western blot. As shown in Figure 1D-E, the three forms of HBsAg are produced and secreted from HuH7-2C8D cells. In the same manner, the two forms of HDAg are detected both in cell lysates and cellular supernatants (Figure 1F-G). Interestingly, the dynamic of intracellular HDAg production demonstrated an initial enrichment in S-HDAg, followed by a switch at day 7 when L-HDAg becomes more expressed in correlation with the timing of HDV replication and the editing of the viral antigenome (Figure 1F), as previously shown in infection systems (Alfaiate *et al.*,

2016). Iodixanol-based density gradient applied to the supernatants of HuH7-2C8 and HuH7-2C8D cells confirmed that HDV RNA was detected in the same fractions as HBsAg (Figure 1H-J), suggesting assembly and secretion of canonical HDV infectious particles. Taken together, our results show that HuH7-2C8D cell line stably produces and secretes HDAg and HBsAg and is as a suitable model for the study of HDV replication and assembly.

HuH7-2C8D cells produce high titer recombinant HDV infectious particles

We tested the infectivity of HDV particles produced in HuH7-2C8D cells using the strategy presented in Figure 2A. HuH7-2C8D cells were plated and cultured in production medium. Supernatants were harvested, pooled, and the titers of the resulting HDV inocula, assessed by qRT-PCR quantification of HDV RNA, were around 10^9 vge/mL. Of note such concentrated HDV viral inocula could be obtained from the classical transfection-based HDV production system only after concentration by PEG precipitation. HuH7-NTCP cells were then seeded and inoculated with HDV particles at increasing Vge per cell. To validate the specificity of infection, HuH7-NTCP were previously treated with a synthetic HBV preS1 peptide that binds to NTCP and inhibits viral entry. HDV infection was assessed by immunodetection of HDAg and RT-qPCR quantification of HDV RNA in infected cells. As shown in Figure 3B-C, inoculation of HuH7-NTCP cells with HuH7-2C8D supernatant leads to the detection of HDAg-positive cells, with HDV RNA levels correlating with the initial virus concentration and with no effect on cell viability as shown by DAPI staining. HDV infection was strongly inhibited by preS1 peptide treatment, validating the specificity of infection. Of note, supernatants derived from HBs-silenced HuH7-2C8D cells (Figure 3D) do not trigger an effective infection in HuH7-NTCP cells (Figure 3D-E). Importantly, shHBs expression has no effect on cell viability, as quantified by the total number of cells at the time of supernatant harvest, and on intracellular HDAg levels (Figure S3). Taken together, our results demonstrated that recombinant HDV particles secreted by HuH7-2C8D cells efficiently infect susceptible cells through a specific infection pathway. HuH7-2C8D cells may therefore serve as a source of large stocks of recombinant virus.

Time-dependent decrease in the infectivity of HDV particles.

As one purpose of this cell line was the large-scale production of recombinant HDV infectious particles, we next aimed to determine the dynamic of virus production in HuH7-2C8D cells. To do so, cells were

seeded, proliferation medium was replaced by production medium after three days, and supernatants were regularly harvested at different time points post medium change (Figure 3A). As shown in Figure 3B, extracellular HBsAg and HDV RNA levels follow more or less the same dynamic. HuH7.5-NTCP, differentiated HepaRG and HuH7-NTCP cells were infected with the different supernatants at an adjusted Vge/cell (Figure 3A). We observed that the levels of infection decreased when cells were inoculated with HuH7-2C8D supernatants collected at late time points (Figure 3C, 3D, 3E), suggesting a time-dependent decrease in HDV particles specific infectivity. Given the dynamic of HDV replication, we hypothesized that during virus production, ADAR-mediated editing of the viral antigenome likely leads to an accumulation of edited versions of the viral genomes that are packaged into *de novo* viral particles. In theory, these are defective viral particles unable to trigger viral replication, given that these edited versions of the genome do not allow the synthesis of S-HDAg, required for viral replication (Lucifora and Delphin, 2020). To test this hypothesis, we assessed the supernatants of HuH7-2C8D cells with a digital droplet PCR (ddPCR) method we recently developed (Verrier *et al.*, 2022). This duplex RT-ddPCR assay allows the independent quantification of both edited and non-edited versions of viral RNA. When applied to the HuH7-2C8 supernatants from different time points post production start, we observed a time-dependent increase in the ratio between edited and non-edited HDV RNA (Figure 3F) that would at least partially explain the decreased in infectivity of viral particles observed in Figure 3C, 3D and 3E. Of note, we believe that this is not a special feature of virions secreted from HuH7-2C8D cells but rather reflects the natural history of HDV particles secretion in a system that do not allow viral propagation and renewal of the initial viral matrix since we also observed an increase in the ratio between edited and non-edited HDV RNA secreted by HDV infected HuH7.5-NTCP (Figure 3G). To circumvent this issue and produce highly concentrated and infectious HDV inocula from HuH7-2C8D cells, we suggest to collect supernatants from HuH7-2C8D cells after 7 days of culture in production media. Indeed, although the virus production slightly decreases among passages, we showed a stable infectivity with such inocula produced from at least 5 consecutive passages of HuH7-2C8D cells (Figure 4).

HuH7-2C8D cells are a useful tool for studies of HDV-host interactions.

We next investigated the possibility of using HuH7-2C8D cells for viral-host interactions studies. First, we confirmed the previously described (Haussecker et al., 2008) intracellular interaction between HDAg

and the cellular helicase MOV10 by co-IP assays (Figure S4). Second, as HuH7-2C8 and HuH7-2C8D cells efficiently secrete HBsAg, we took advantage of these cells to analyze the interplay between HBsAg and macrophages which have been suggested to play a functional role in pathogenesis of liver disease. We previously showed that the presence of HBV modulates the secretion of cytokines, notably by decreasing IL-1β secretion in macrophages, using a co-culture model of monocyte-derived macrophages (MDMs) and HepAD38 cells (Faure-Dupuy et al., 2019). More recently and using the same co-culture model, we associated the aforementioned modulations with HBsAg, as already suggested by others (Delphin *et al.*, 2021; Wang et al., 2013; Zannetti et al., 2016). In order to validate this hypothesis using our new cellular model, HuH7, HuH7-2C8, and HuH7-2C8D cells were cultured during monocyte differentiation into M1-MDMs as illustrated in Figure 5A. After stimulation of M1-MDMs with LPS, cytokine secretion was assessed by ELISA. As shown in Figure 5B, co-culture of monocytes (during differentiation into M1-MDMs) with HuH7-2C8 resulted in a decreased production of IL-6 and IL-1β upon LPS stimulation. The same observation was made from HuH7-2C8D co-cultures (Figure 5C). Taken together, we confirmed the ability of HBsAg in the presence of HDV virions to impair the secretion of cytokines from macrophages. Additionally, we confirmed the suitability of our cell culture system for the study of many steps of virus host-interactions.

FTI treatment decreases virion secretion and infectivity

Finally, we evaluated the ability of HuH7-2C8D cells to be a suitable model for the study of the mode of action of antivirals targeting HDV assembly and release. As FTIs, such as lonafarnib, have been shown to inhibit HDV assembly by impairing L-HDAg prenylation, we treated HuH7-2C8D cells with FTI-277 and assessed the viral parameters at different time points post treatment as well as the infectivity of the secreted particles (Figure 6A). We observed an intracellular accumulation of HDV RNA upon FTI-277 treatment, as previously reported by several groups including ours (Alfaiate *et al.*, 2016; Lempp *et al.*, 2019; Sato *et al.*, 2004; Verrier *et al.*, 2022) (Figure 6B). While secreted HBsAg levels were not affected by FTI-277, a robust decrease in secreted HDV RNA was observed (Figure 6C) as expected. Recently, we demonstrated a second antiviral effect of FTI-277, by decreasing not only the number of secreted particles, but also the infectivity of the remaining virions that are produced upon antiviral treatment (Verrier *et al.*, 2022). To validate this hypothesis, HuH7-2C8D cells were seeded one day prior to treatment with FTI-277 for 9 days. An expected significant decrease in secreted HDV RNA levels was

observed compared to DMSO-treated cells (Figure 6D) in absence of any effect on HBsAg levels (Figure 6E) and cell viability (Figure S5A). Supernatants from both conditions were then used to infect naive HuH7-NTCP cells at an adjusted Vge/cell of 100. As shown in Figure 6E, a marked decrease in virus infection was observed in cells infected with FTI-277-treated supernatants, demonstrating a strong reduction of virion infectivity upon FTI treatment. Of note, we excluded that the decrease of infectivity observed might be due to mis-quantification of our viral inocula since we obtained linear quantifications (Figure S5B). Interestingly, we validated this result using lonafarnib, which seems more efficient than FTI-277 at inhibiting L-HDAg-mediated viral secretion (Figure 6F). A similar decrease in virion infectivity in lonafarnib-treated cells compared to FTI-277 was observed at a low MOI of 25 Vge/cell (Figure 6G). Taken together, our results validated the HuH7-2C8D cell line as a suitable model for the study of virion assembly and release as well as the screening of antivirals, and confirmed the dual antiviral activity of FTI on HDV infection.

DISCUSSION

Chronic hepatitis D is f the most severe form of chronic viral hepatitis associated with liver disease progression to liver failure and hepatocellular carcinoma. Efficient and safe therapies curing HDV infection and leading to an improvement of patients' outcome are needed. In this context, a comprehensive characterization of HDV-host interactions is required for the characterization of new antiviral targets. Importantly, HDV assembly and release are still poorly understood. Here, we propose a novel stable cell line allowing both the production of large scale of viral particles and the study of critical steps of the life cycle, including replication, interactions with cellular partners, viral assembly and release. Notably, we demonstrated the value of our model for the study of interplay between HDV-infected hepatic cells and macrophages (without cell contact), by confirming the ability of HBsAg to inhibit the secretion of IL-1β and IL-6 by macrophages. Interestingly, HuH7-2C8D cells allow the production of highly concentrated HDV inocula around 10^9 vge/mL that can even reach 10^{10} vge/mL after PEG precipitation. 1mL of such a virus stock can be used to infect up to 10^4 wells of susceptible cells from 96-well plates, considering 10^4 cells/well and a multiplicity of infection of 100 vge/cell. This study further advances HDV infection and production models (Lempp *et al.*, 2019; Ni et al., 2019; Verrier *et al.*, 2016a; Verrier *et al.*, 2020; Yan *et al.*, 2012) by providing a source of highly infectious HDV particles suitable for high-throughput mechanistic studies and discovery of host-dependency factors and

novel antivirals. Of note, the HuH7-END cell line was recently developed with a similar strategy but including in addition the expression of the HDV receptor NTCP (Ni *et al.*, 2019). We report here a higher range of HDV particles production in HuH7-2C8D than the one reported in HuH7-END. However, since quantification of HDV copy numbers could be dramatically different between laboratories (Le Gal et al., 2016), the two cell lines should compared side-by-side regarding virus production to draw any further conclusions. Importantly, HuH7 cell line seems to be particularly adapted to the production of HDV-replicating cells, probably because no activation of the innate immunity, usually triggered by the sensing of the HDV genome by MDA5 is observed in this cell line (Zhang et al., 2018).

When applied to study key aspects of the HDV life cycle, HuH7-2C8D cells allowed to confirm the dual antiviral activity of FTIs on HDV infection. FTIs including lonafarnib, currently evaluated in clinical trial, are known to inhibit L-HDAg prenylation and thus the production of HDV virions. By inhibiting L-HDAg prenylation, FTIs also impair the ability of L-HDAg to inhibit viral replication (Sato *et al.*, 2004). As a consequence, FTI treatment leads to an temporary accumulation of intracellular RNA as previously described (Alfaiate *et al.*, 2016; Lempp *et al.*, 2019; Sato *et al.*, 2004; Verrier *et al.*, 2022) and confirmed in this study, although the pool of HDV RNA is eventually decreasing even in presence of FTI (Figure 6B). As ADAR constantly edits the antigenome throughout the replication, this accumulation affects more and more edited versions of HDV RNA. Recently, we demonstrated that this modulation of edited / non-edited ratio was associated to a loss of infectivity of HDV particles, probably because particles packaging an edited version of the genome are unable to trigger viral replication (Verrier *et al.*, 2022). Here, we confirmed this result, exemplifying the usefulness of our cell line to characterize the mechanism of action of antiviral molecules. Moreover, we observed that, even in absence of treatment, the modulation of edited versus non-edited ratio is associated with a decrease in the infectivity of viral particles that are produced. This observation reinforces the hypothesis of the inability of edited genome-containing HDV particles to infect naive cells due to the lack of S-HDAg expression. Importantly, the infectivity drop is more pronounced than the increase in edited genome fraction in the supernatant, suggesting that a complex process putatively involving other mechanisms explains the loss of infectivity of viral particles with time. Notably, although it has been demonstrated that L-HDAg inhibits the synthesis of HDV antigenome only when present in large excess (Modahl and Lai, 2000), we cannot exclude that cells may become infected by multiple viruses, leading to an inhibition of HDV replication by the L-HDAg coding genomes, which become predominant with time (Figure 3F).

In conclusion, we established a stable cell line enabling the production of large quantity of viral particles for high-throughput studies in infection models. To date, recombinant HDV production relies on co-transfection of cells with HBsAg-encoding plasmid and HDV-encoding plasmid (Sureau *et al.*, 1994). The HuH7-2C8D cell line provides a fast and convenient method to produce virus, overcoming the costs and time issues with transient transfection methods. Moreover, as an immortalized cell line, HuH7-2C8D cells should be suitable for high-throughput small molecule and genetic screens for the characterization of host factors involved in HDV replication, assembly and release, that would be complementary to the existing datasets characterizing HDV replication in mono-infection models (in absence of HBsAg) (for instance (Verrier *et al.*, 2020)). Taken together, this will improve our understanding of HDV molecular virology.

Author Contributions: F.P, T.F.B and E.R.V. initiated the study. E.R.V. supervised research. C.B. produced the cell lines. C.B., J.L., M.D., L.H., M.H., C.P., and K.G. characterized the cell lines and performed the validation experiments. J.L. performed the RT-ddPCR experiments. M.D. performed the co-culture experiments. C.B., J.L., M.D., E.S., L.H., M.H., C.P., C.S., D.D., F.P., T.F.B., and E.L.V. analyzed the data. E.R.V. wrote the manuscript and J.L., M.D., E.S., F.P., D.D., and T.F.B. reviewed it. All the authors approved the manuscript. C.B. and J.L. equally contributed to this study as first author.

Funding: This work of the Interdisciplinary Thematic Institute IMCBio, as part of the ITI 2021-2028 program of the University of Strasbourg, CNRS and Inserm, was supported by IdEx Unistra (ANR-10-IDEX-0002), and by SFRI-STRAT'US project (ANR 20-SFRI-0012) and EUR IMCBio (ANR-17-EURE-0023) under the framework of the French Investments for the Future Program. E.R.V acknowledges fundings from Inserm, the Agence Nationale de Recherches sur le Sida et les Hépatites Virales (ANRS, grant number ECTZ171594), and the French National Research Agency (ANR, grant number ANR-21-CE15-0035-01 DELTArget). J.L. acknowledges fundings from Inserm, CNRS, University of Lyon, and ANRS (grant number ECTZ172540). T. F. B and E. R. V. received funding from Janssen Pharmaceutica as part of the VLAIO project ABDeCo (HBC.2017.0895). T. F. B acknowledges funding from the European Union (EU ERC-AdG-2014-HEPCIR #671231 and ARC TheraHCC2.0 IHU201901299.

Data Availability Statement: The original data from this study are available through the corresponding author upon reasonable request.

Acknowledgments: We thank Professor Stephan Urban (University Hospital Heidelberg, Heidelberg, Germany) and Doctor John Taylor (Fox Chase Cancer Center, Philadelphia, PA, USA) for having kindly provided the pLX304-HB2.7 and pSVLD3 plasmids, respectively. We thank Professor Fabien Zoulim and Doctor Barbara Testoni (CRCL, Lyon, France) for the use of the ddPCR device. We acknowledge Emilie Crouchet (Inserm UMR_S1110, Strasbourg, France) for excellent technical support, and Anne Zeter (Inserm UMR_S1110, Strasbourg, France) and Annie Tu (SATT Conectus Alsace, Illkirch, France) for excellent administrative support.

Conflicts of Interest: T. F. B and E. R. V. received funding from Janssen Pharmaceutica as part of the VLAIO project ABDeCo (HBC.2017.0895). E.S. and F.P. are employees of Janssen Research and Development and may be Johnson & Johnson stockholders.

REFERENCES

Alfaiate, D., Lucifora, J., Abeywickrama-Samarakoon, N., Michelet, M., Testoni, B., Cortay, J.C., Sureau, C., Zoulim, F., Deny, P., and Durantel, D. (2016). HDV RNA replication is associated with HBV repression and interferon-stimulated genes induction in super-infected hepatocytes. Antiviral Res *136*, 19-31. 10.1016/j.antiviral.2016.10.006.

Chen, P.J., Kuo, M.Y., Chen, M.L., Tu, S.J., Chiu, M.N., Wu, H.L., Hsu, H.C., and Chen, D.S. (1990). Continuous expression and replication of the hepatitis delta virus genome in Hep G2 hepatoblastoma cells transfected with cloned viral DNA. Proc Natl Acad Sci U S A *87*, 5253-5257. 10.1073/pnas.87.14.5253.

Delphin, M., Faure-Dupuy, S., Isorce, N., Rivoire, M., Salvetti, A., Durantel, D., and Lucifora, J. (2021). Inhibitory Effect of IL-1beta on HBV and HDV Replication and HBs Antigen-Dependent Modulation of Its Secretion by Macrophages. Viruses *14*. 10.3390/v14010065.

Eller, C., Heydmann, L., Colpitts, C.C., El Saghire, H., Piccioni, F., Juhling, F., Majzoub, K., Pons, C., Bach, C., Lucifora, J., et al. (2020). A genome-wide gain-of-function screen identifies CDKN2C as a HBV host factor. Nat Commun *11*, 2707. 10.1038/s41467-020-16517-w.

Faure-Dupuy, S., Delphin, M., Aillot, L., Dimier, L., Lebosse, F., Fresquet, J., Parent, R., Matter, M.S., Rivoire, M., Bendriss-Vermare, N., et al. (2019). Hepatitis B virus-induced modulation of liver

macrophage function promotes hepatocyte infection. J Hepatol *71*, 1086-1098. 10.1016/j.jhep.2019.06.032.

Gripon, P., Rumin, S., Urban, S., Le Seyec, J., Glaise, D., Cannie, I., Guyomard, C., Lucas, J., Trepo, C., and Guguen-Guillouzo, C. (2002). Infection of a human hepatoma cell line by hepatitis B virus. Proc Natl Acad Sci U S A *99*, 15655-15660. 10.1073/pnas.232137699.

Haussecker, D., Cao, D., Huang, Y., Parameswaran, P., Fire, A.Z., and Kay, M.A. (2008). Capped small RNAs and MOV10 in human hepatitis delta virus replication. Nat Struct Mol Biol *15*, 714-721. 10.1038/nsmb.1440.

Herrscher, C., Pastor, F., Burlaud-Gaillard, J., Dumans, A., Seigneuret, F., Moreau, A., Patient, R., Eymieux, S., de Rocquigny, H., Hourioux, C., et al. (2020a). Hepatitis B virus entry into HepG2-NTCP cells requires clathrin-mediated endocytosis. Cell Microbiol *22*, e13205. 10.1111/cmi.13205.

Herrscher, C., Roingeard, P., and Blanchard, E. (2020b). Hepatitis B Virus Entry into Cells. Cells *9*. 10.3390/cells9061486.

Heuschkel, M.J., Baumert, T.F., and Verrier, E.R. (2021). Cell Culture Models for the Study of Hepatitis D Virus Entry and Infection. Viruses *13*. 10.3390/v13081532.

Le Gal, F., Brichler, S., Sahli, R., Chevret, S., and Gordien, E. (2016). First international external quality assessment for hepatitis delta virus RNA quantification in plasma. Hepatology *64*, 1483-1494. 10.1002/hep.28772.

Lebosse, F., Inchauspe, A., Locatelli, M., Miaglia, C., Diederichs, A., Fresquet, J., Chapus, F., Hamed, K., Testoni, B., and Zoulim, F. (2020). Quantification and epigenetic evaluation of the residual pool of hepatitis B covalently closed circular DNA in long-term nucleoside analogue-treated patients. Sci Rep *10*, 21097. 10.1038/s41598-020-78001-1.

Lempp, F.A., Schlund, F., Rieble, L., Nussbaum, L., Link, C., Zhang, Z., Ni, Y., and Urban, S. (2019). Recapitulation of HDV infection in a fully permissive hepatoma cell line allows efficient drug evaluation. Nat Commun *10*, 2265. 10.1038/s41467-019-10211-2.

Lucifora, J., and Delphin, M. (2020). Current knowledge on Hepatitis Delta Virus replication. Antiviral Res *179*, 104812. 10.1016/j.antiviral.2020.104812.

Lupberger, J., Zeisel, M.B., Xiao, F., Thumann, C., Fofana, I., Zona, L., Davis, C., Mee, C.J., Turek, M., Gorke, S., et al. (2011). EGFR and EphA2 are host factors for hepatitis C virus entry and possible targets for antiviral therapy. Nat Med *17*, 589-595. 10.1038/nm.2341.

Modahl, L.E., and Lai, M.M. (2000). The large delta antigen of hepatitis delta virus potently inhibits genomic but not antigenomic RNA synthesis: a mechanism enabling initiation of viral replication. J Virol *74*, 7375-7380. 10.1128/jvi.74.16.7375-7380.2000.

Ni, Y., Lempp, F.A., Mehrle, S., Nkongolo, S., Kaufman, C., Falth, M., Stindt, J., Koniger, C., Nassal, M., Kubitz, R., et al. (2014). Hepatitis B and D viruses exploit sodium taurocholate co-transporting polypeptide for species-specific entry into hepatocytes. Gastroenterology *146*, 1070-1083. 10.1053/j.gastro.2013.12.024.

Ni, Y., Zhang, Z., Engelskircher, L., Verch, G., Tu, T., Lempp, F.A., and Urban, S. (2019). Generation and characterization of a stable cell line persistently replicating and secreting the human hepatitis delta virus. Sci Rep *9*, 10021. 10.1038/s41598-019-46493-1.

Sato, S., Cornillez-Ty, C., and Lazinski, D.W. (2004). By inhibiting replication, the large hepatitis delta antigen can indirectly regulate amber/W editing and its own expression. J Virol *78*, 8120-8134. 10.1128/JVI.78.15.8120-8134.2004.

Schulze, A., Gripon, P., and Urban, S. (2007). Hepatitis B virus infection initiates with a large surface protein-dependent binding to heparan sulfate proteoglycans. Hepatology *46*, 1759-1768. 10.1002/hep.21896.

Sureau, C., Guerra, B., and Lee, H. (1994). The middle hepatitis B virus envelope protein is not necessary for infectivity of hepatitis delta virus. J Virol *68*, 4063-4066. 10.1128/JVI.68.6.4063-4066.1994.

Sureau, C., and Negro, F. (2016). The hepatitis delta virus: Replication and pathogenesis. J Hepatol *64*, S102-S116. 10.1016/j.jhep.2016.02.013.

Turon-Lagot, V., Saviano, A., Schuster, C., Baumert, T.F., and Verrier, E.R. (2020). Targeting the Host for New Therapeutic Perspectives in Hepatitis D. J Clin Med *9*, 222. 10.3390/jcm9010222.

Urban, S., Neumann-Haefelin, C., and Lampertico, P. (2021). Hepatitis D virus in 2021: virology, immunology and new treatment approaches for a difficult-to-treat disease. Gut *70*, 1782-1794. 10.1136/gutjnl-2020-323888.

Verrier, E.R., Colpitts, C.C., Bach, C., Heydmann, L., Weiss, A., Renaud, M., Durand, S.C., Habersetzer, F., Durantel, D., Abou-Jaoude, G., et al. (2016a). A targeted functional RNA interference screen uncovers glypican 5 as an entry factor for hepatitis B and D viruses. Hepatology *63*, 35-48. 10.1002/hep.28013.

Verrier, E.R., Colpitts, C.C., Bach, C., Heydmann, L., Zona, L., Xiao, F., Thumann, C., Crouchet, E., Gaudin, R., Sureau, C., et al. (2016b). Solute Carrier NTCP Regulates Innate Antiviral Immune Responses Targeting Hepatitis C Virus Infection of Hepatocytes. Cell Rep *17*, 1357-1368. 10.1016/j.celrep.2016.09.084.

Verrier, E.R., Salvetti, A., Pons, C., Michelet, M., Rivoire, M., Baumert, T.F., Durantel, D., and Lucifora, J. (2022). Loss of hepatitis D virus infectivity upon farnesyl transferase inhibitor treatment associates with increasing RNA editing rates revealed by a new RT-ddPCR method. Antiviral Res *198*, 105250. 10.1016/j.antiviral.2022.105250.

Verrier, E.R., Weiss, A., Bach, C., Heydmann, L., Turon-Lagot, V., Kopp, A., El Saghire, H., Crouchet, E., Pessaux, P., Garcia, T., et al. (2020). Combined small molecule and loss-of-function screen uncovers estrogen receptor alpha and CAD as host factors for HDV infection and antiviral targets. Gut *69*, 158-167. 10.1136/gutjnl-2018-317065.

Wang, S., Chen, Z., Hu, C., Qian, F., Cheng, Y., Wu, M., Shi, B., Chen, J., Hu, Y., and Yuan, Z. (2013). Hepatitis B virus surface antigen selectively inhibits TLR2 ligand-induced IL-12 production in monocytes/macrophages by interfering with JNK activation. J Immunol *190*, 5142-5151. 10.4049/jimmunol.1201625.

Yan, H., Zhong, G., Xu, G., He, W., Jing, Z., Gao, Z., Huang, Y., Qi, Y., Peng, B., Wang, H., et al. (2012). Sodium taurocholate cotransporting polypeptide is a functional receptor for human hepatitis B and D virus. Elife *1*, e00049. 10.7554/eLife.00049.

Zannetti, C., Roblot, G., Charrier, E., Ainouze, M., Tout, I., Briat, F., Isorce, N., Faure-Dupuy, S., Michelet, M., Marotel, M., et al. (2016). Characterization of the Inflammasome in Human Kupffer Cells in Response to Synthetic Agonists and Pathogens. J Immunol *197*, 356-367. 10.4049/jimmunol.1502301.

Zhang, Z., Filzmayer, C., Ni, Y., Sultmann, H., Mutz, P., Hiet, M.S., Vondran, F.W.R., Bartenschlager, R., and Urban, S. (2018). Hepatitis D virus replication is sensed by MDA5 and induces IFN-beta/lambda responses in hepatocytes. J Hepatol *69*, 25-35. 10.1016/j.jhep.2018.02.021.

Figure legends:

Figure 1. Approach and virological characterization of the HuH7-2C8D cell line. **A.** Experimental strategy. HuH7 cells were first transduced with pLX304-HB2.7 lentiviral vector. From the HuH7.HB2.7 cell pool, HuH7-2C8 clone was isolated, expanded and transfected with HDV-expressing pSVLD3-neo plasmid, leading to the production of the HuH7-2C8D pool cell line. **B.** Intracellular HBsAg levels in the indicated cell lines assessed by flow cytometry. One representative experiment is shown. **C.** Extracellular HBsAg expression levels determined by CLIA in the supernatants of the different cell lines. Results are expressed as means ± SD secreted HBsAg (UI/mL) from three independent experiments (n=15). **D-E.** Intracellular (**D**) and extracellular (**E**) HBsAg expression level from HuH7-2C8D cells assessed by Western blot. HuH7-2C8D cells were seeded and supernatants were harvested and cell lysed at the indicated time points post seeding. For intracellular HBsAg levels, β-tubulin expression was detected in parallel as a control (**D**). One representative blot is shown. **F-G.** Intracellular (**F**) and extracellular (**G**) HDAg expression level from HuH7-2C8D cells assessed by Western blot. HuH7-2C8D cells were seeded, supernatants were harvested, and cell were lysed at the indicated time points post seeding. For intracellular HDAg levels, β-actin expression was detected in parallel as a control (**D**). One representative blot is shown. **H-J**. Iodixanol-based density gradient. Supernatant from HuH7-2C8 (**H**) and HuH7-2C8D (**I**) cells were concentrated with a 30% sucrose cushion and purified through a 10-45% iodixanol density gradient. Ten fractions were collected. HBsAg levels in each fraction were assessed by CLIA. Alternatively, total RNA was extracted and HDV RNA levels in each fraction were quantified by RT-qPCR. 200 µL of each fraction were weighted to assess the density (**J**). One representative experiment out of three independent experiments is shown. *** $p < 0.001$.

Figure 2. Infection of HuH7-NTCP cells with HDV-containing supernatants from HuH7-2C8D cells. **A.** Experimental strategy. HuH7-2C8D cells were seeded and cultured in production medium. Supernatants were regularly harvested, pooled, and HDV RNA was quantified by RT-qPCR. **B-C**. HuH7-NTCP cells were seeded one day prior to incubation or not for 1h with preS1 peptide at 37°C. HuH7-NTCP were then inoculated with HDV-containing supernatants at the indicated Vge/cell. HDV infection was assessed at 6 days post infection (dpi) by intracellular immunodetection of HDAg. The number of HDAg-positive cells was quantified using a plate cytometer (**B**). Results are expressed as means ± SD % HDV infection compared to control HuH7-NTCP cells infected with HDV at 1000 Vge/cell (set at 100%) from

three independent experiments (n=9). Representative IF pictures for each condition are presented (**C**). scale bar: 100 µm. **D-F**. Impact of shHBs expression on production of HDV infectious particles. HuH7-2C8D cells were seeded one day prior to transduction with shHBs- or shCtrl-expressing lentiviral vector. Cells were selected with puromycin and supernatants were harvested. shRNA efficacy was assessed by quantification of HBsAg by CLIA (**D**). Results are expressed as means ± SD % HBsAg secretion compared to shCtrl-treated cells (set at 100%) from three independent experiments (n=10). HuH7-NTCP cells were then inoculated with the supernatants at adjusted volume. HDV infection was assessed at 6 dpi by RT-qPCR quantification of HDV RNA (**E**). Results are expressed as means ± SD % HDV RNA compared to HuH7-NTCP infected with supernatant from shCtrl-treated HuH7-2C8D cells (set at 100%) from three independent experiments (n=8). Alternatively, infection was assessed by quantification of HDAg-positive cells by IF using a plate cytometer (**E-F**). Results are expressed as means ± SD % HDAg-positive cells compared to HuH7-NTCP infected with supernatant from shCtrl-treated HuH7-2C8D cells (set at 100%) from three independent experiments (n=10). Representative IF pictures are presented. NT: non transfected cells. scale bar: 100 µm. *** $p < 0.001$.

Figure 3. Dynamic of HDV production in HuH7-2C8D cells. **A.** Experimental strategy. HuH7-2C8D cells were seeded three days prior to replacement by production medium. Supernatants were then regularly harvested and viral parameters were assessed (**B**). Results are expressed as means ± SD % secreted HDV RNA compared to HDV RNA at day 11 (maximum, set at 100%) from three independent experiments (n=18) and as means ± SD % HBsAg levels compared HBsAg at day 14 (maximum, set at 100%) from three independent experiments (n=9). Supernatants from the indicated time points were used to infect HuH7.5-NTCP (**C**), dHepaRG (**D**), or HuH7-NTCP (**E**) cells at an adjusted Vge/cell of 100. HDV infection was assessed at 6 dpi by quantification of intracellular HDV RNA by RT-qPCR. Results are expressed as means ± SD % HDV RNA compared to cells infected with DMSO-treated supernatant (both set at 100%) from three independent experiments (n=9). **F.** Supernatants used to infect HuH7-NTCP in (**E**) were subjected to RT-ddPCR method allowing the independent quantification of edited and non-edited version of HDV RNA. Results are expressed as fractions of edited (E) and non-edited (NE) HDV RNA from three independent experiments (n=9). **G.** To confirm this results, supernatants from HBV/HDV-coinfected HuH7.5-NTCP cells were also were subjected to RT-ddPCR. Results are expressed as fractions of edited (E) and non-edited (NE) HDV RNA from one experiment (n=2).

Figure 4. Dynamic of HDV production upon successive passages of HuH7-2C8D cells. **A.** Experimental design. HuH7-2C8D cells cultured in culture medium were plated at each passage (P), every 3 to 4 days, and cultured in production medium. Seven days after plating, supernatants were harvested and secreted HDV RNA was assessed by RT-qPCR. 5 successive passages were studied. Results are expressed as means ± SD % secreted HDV RNA compared to the first plating (P1, set at 100%) from three independent experiments (n=9). A supernatant from HuH7-2C8 cells, not expressing the HDV genome, was used as a control (n=3). **C.** Supernatants from each passage were used to infect HuH7-NTCP cells at an adjusted Vge/cell of 100. HDV infection was assessed 6 dpi by quantification of HDV-positive cells by IF. Results are expressed as means ± SD % HDV-infected cells from one experiment (n = 3).

Figure 5. HBsAg secretion inhibits cytokine secretion by macrophages. A. Experimental strategy. HuH7, HuH7-2C8, and HuH7-2C8D cells were co-cultured with monocytes, which were differentiated in M1-MDMs for 6 days using GM-CSF. M1-MDMs were then stimulated with LPS and cytokine secretion was assessed by ELISA 24h later. (B-C). Results are expressed as means ± SD ratio IL-6 and IL-1β secretion levels normalized to HuH7 conditions (control condition, set at 1) from two independent experiments (**B**, n=8) and four independent experiments (**C**, n=16, including 8 control points similar to **B**). ** $p < 0.01$; *** $p < 0.001$

Figure 6: FTI treatment inhibits virus production and infectivity. **A.** Experimental strategy. HuH7-2C8D cells were seeded three days prior to treatment with FTI-277 at 10µM. Supernatants were harvested and cells were lysed at different time points and viral parameters were assessed. Intracellular HDV RNA was assessed by RT-qPCR (**B**). Results are expressed as means ± SD % HDV RNA compared to HDV RNA in control cells at day 3 post treatment start (set at 100%) from one experiment (n=4). Extracellular HDV RNA and HBsAg were assessed by RT-qPCR and CLIA, respectively (**C**). Results are expressed as means ± SD secreted HDV RNA copies/µL (n=2) and as HBsAg concentration (UI/mL, one experiment is shown). **D-E.** FTI-277 affects virion infectivity. HuH7-2C8D cells were seeded one day prior to treatment with FTI-277 at 10µM or with DMSO as a control for 9 days. Supernatants were harvested and viral parameters were assessed (**D**). Results are expressed as means ± SD secreted

HDV RNA copies/µL from three independent experiments (n=9) and as % HBsAg levels compared to DMSO-treated cells (set at 100%) from three independent experiments (n=9). HuH7-NTCP cells were then infected with the supernatants from DMSO- and FTI-277-treated cells at 100 Vge/cell (E). HDV infection was assessed at 6 dpi by quantification of intracellular HDV RNA by RT-qPCR and HDAg-positive cells using a plate cytometer. Results are expressed as means ± SD % HDV RNA or as % HDAg-positive cells compared to cells infected with DMSO-treated supernatant (both set at 100%) from three independent experiments (n=9). ** $p < 0.01$; *** $p < 0.001$.

Figure 1

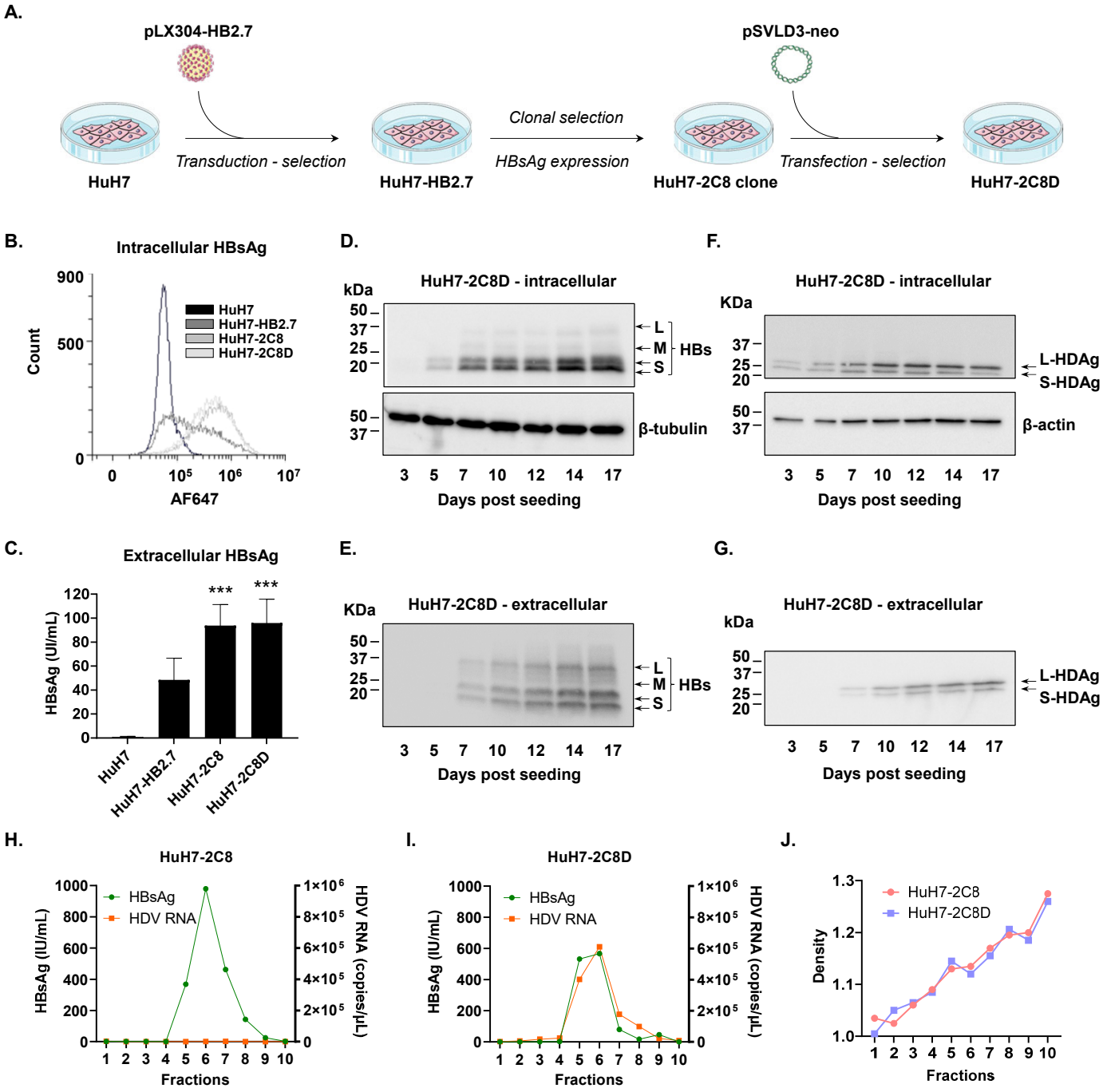

Figure 2

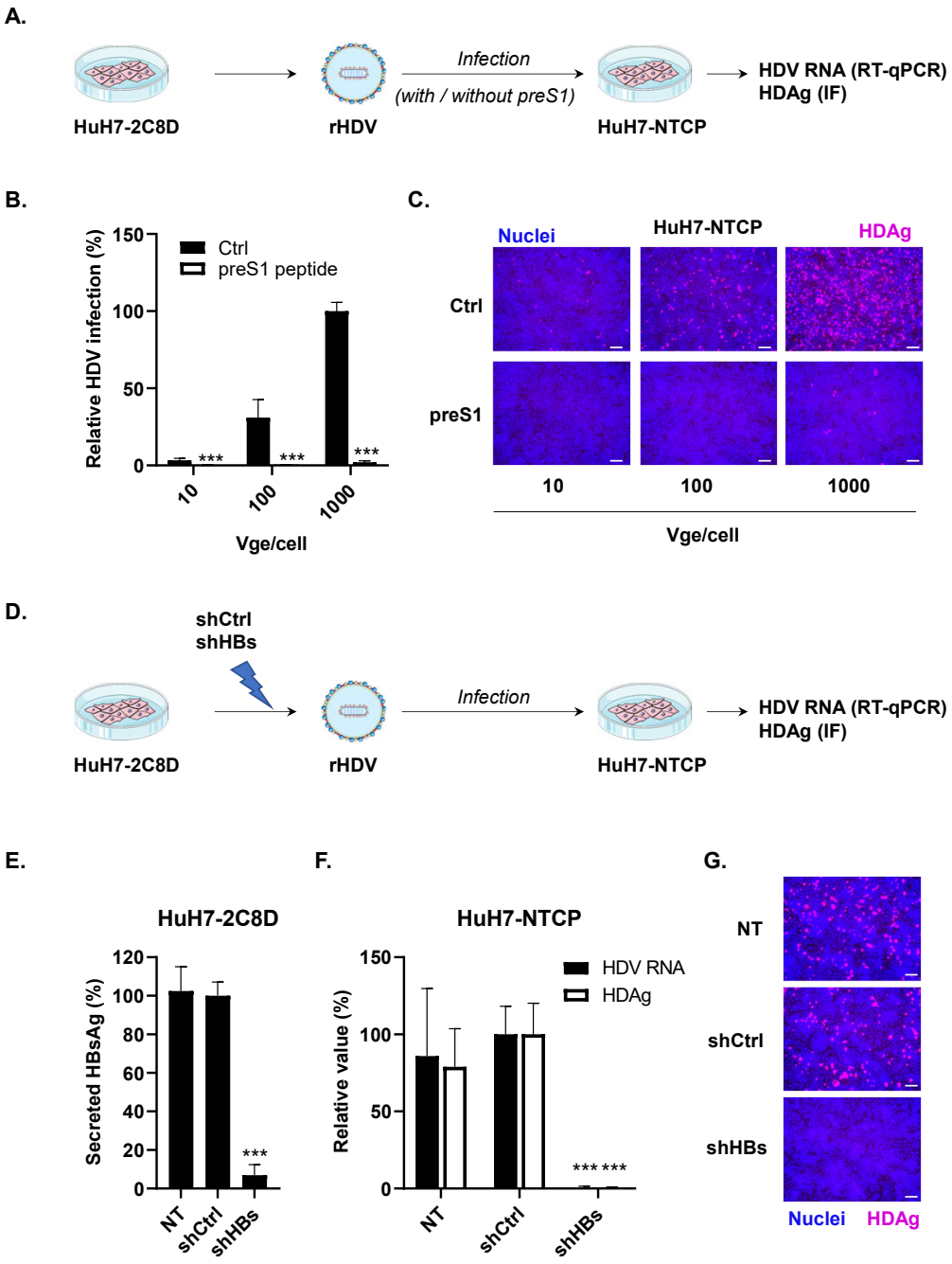

Figure 3

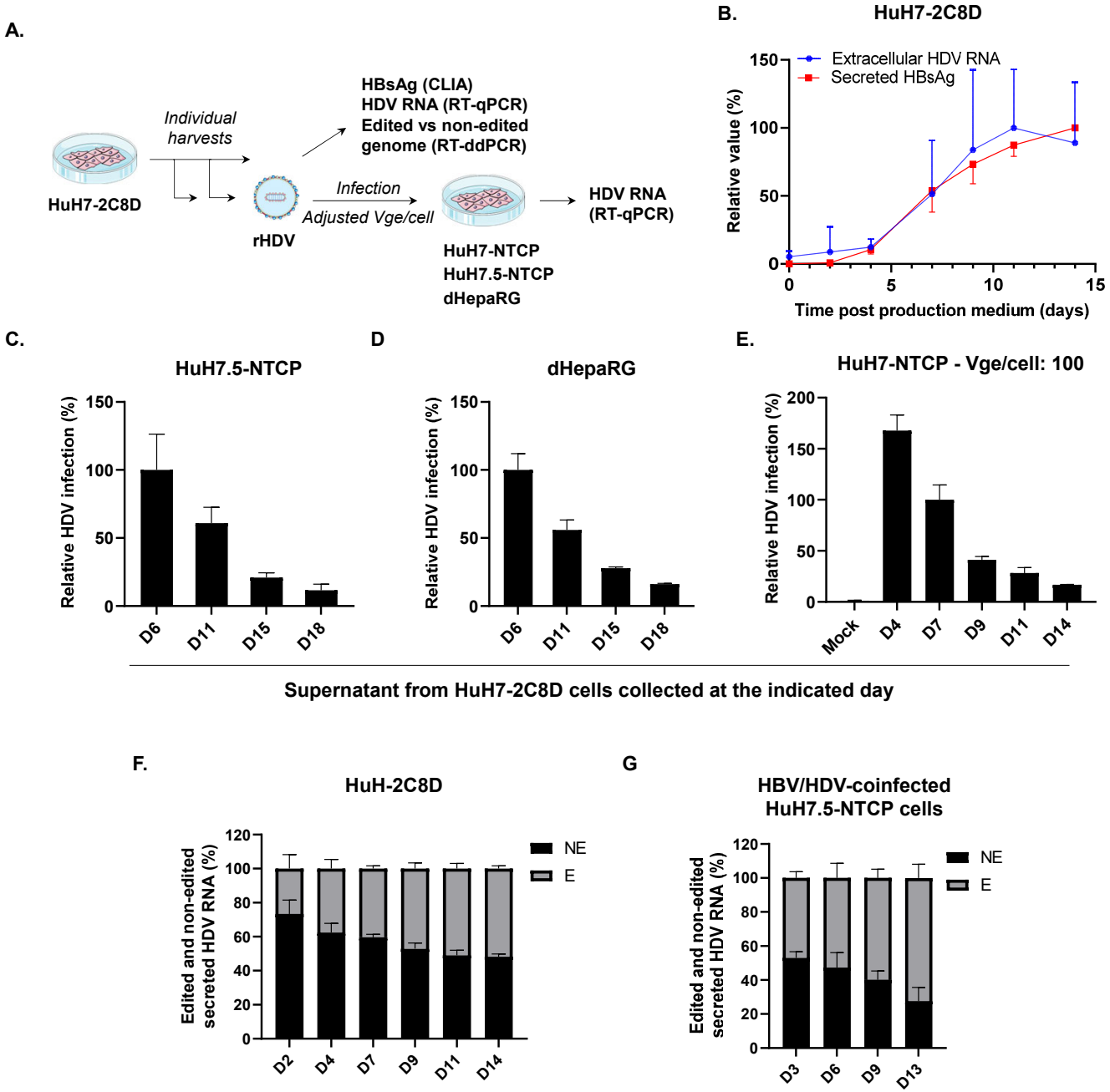

Figure 4

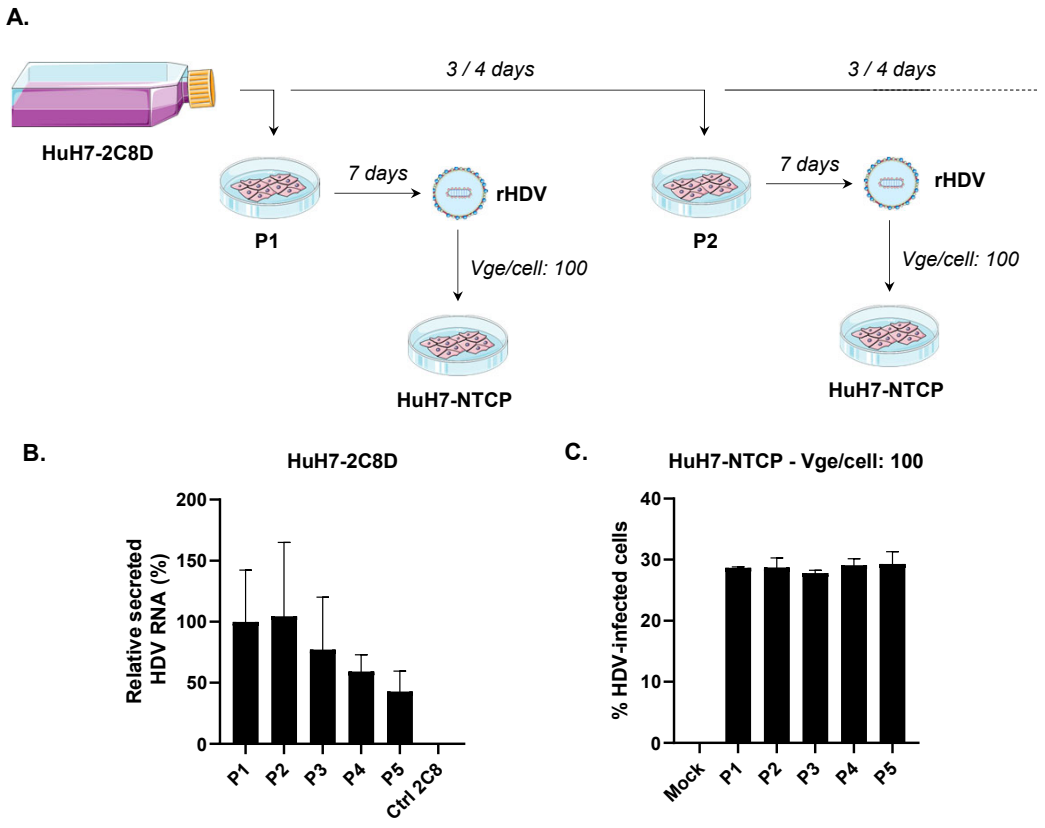

Figure 5

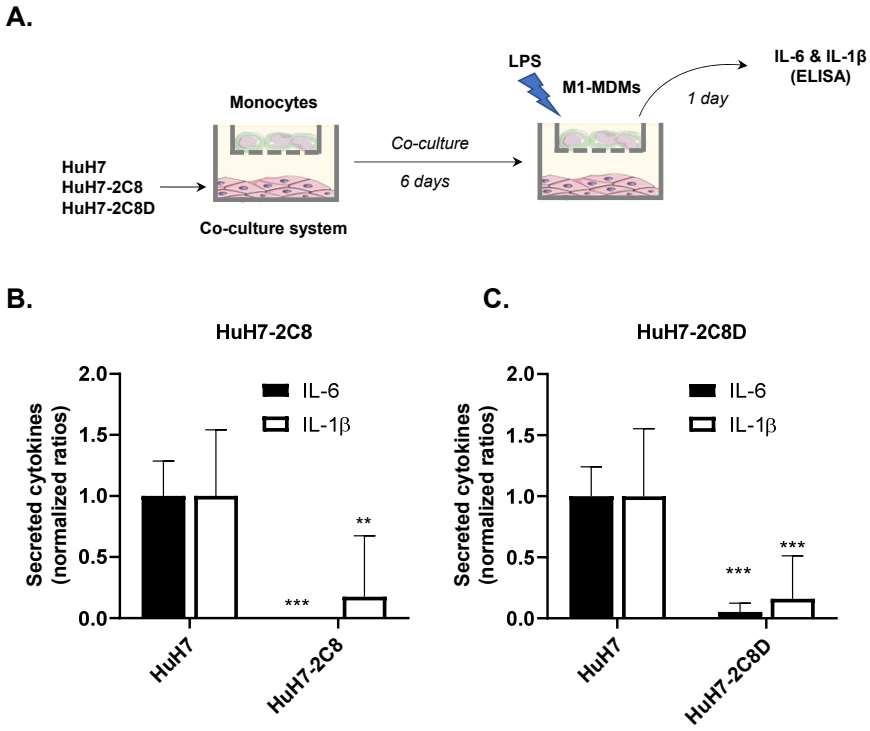

Figure 6